Journal of Controlled Release 308 (2019) 109–118

Contents lists available at ScienceDirect

Journal of Controlled Release

journal homepage: www.elsevier.com/locate/jconrel

Peptide-guided nanoparticles for glioblastoma targeting

Pille Säälik[a,1], Prakash Lingasamy[a,1], Kadri Toome[a], Ignacio Mastandrea[b], Liat Rousso-Noori[b], Allan Tobi[a], Lorena Simón-Gracia[a], Hedi Hunt[a], Päärn Paiste[c], Venkata Ramana Kotamraju[d], Gabriele Bergers[e], Toomas Asser[f], Tõnu Rätsep[f], Erkki Ruoslahti[d,g], Rolf Bjerkvig[h], Dinorah Friedmann-Morvinski[b,**], Tambet Teesalu[a,d,g,*]

[a] Laboratory of Cancer Biology, Institute of Biomedicine, Centre of Excellence for Translational Medicine, University of Tartu, Tartu, Estonia
[b] Sagol School of Neuroscience, Department of Biochemistry and Molecular Biology, The George S. Wise Faculty of Life Sciences, Tel Aviv University, Israel
[c] Department of Geology, University of Tartu, Tartu, Estonia
[d] Cancer Research Center, Sanford Burnham Prebys Medical Discovery Institute, La Jolla, California, USA
[e] Laboratory for Tumor Microenvironment and Therapeutic Resistance, VIB-KU Leuven Center for Cancer Biology, Leuven, Belgium
[f] Department of Neurosurgery, Tartu University Hospital, Tartu, Estonia
[g] Center for Nanomedicine and Department of Cell, Molecular and Developmental Biology, University of California Santa Barbara, Santa Barbara, CA, USA
[h] Department of Biomedicine, University of Bergen, Bergen, Norway

ARTICLE INFO

Keywords:
Homing peptide
C-end rule
TT1 peptide
Neuropilin-1
p32
Nanoworms
Glioblastoma

ABSTRACT

Tumor-selective drug conjugates can potentially improve the prognosis for patients affected by glioblastoma (GBM) – the most common and malignant type of brain cancer with no effective cure.

Here we evaluated a novel tumor penetrating peptide that targets cell surface p32, LinTT1 (AKRGARSTA), as a GBM targeting ligand for systemically-administered nanoparticles. LinTT1-functionalization increased tumor homing of iron oxide nanoworms (NWs) across a panel of five GBM models ranging from infiltratively-disseminating to angiogenic phenotypes. LinTT1-NWs homed to CD31-positive tumor blood vessels, including to transdifferentiated endothelial cells, and showed co-localization with tumor macrophages and lymphatic vessels. LinTT1 functionalization also resulted in increased GBM delivery of other types of systemically-administered nanoparticles: silver nanoparticles and albumin-paclitaxel nanoparticles. Finally, LinTT1-guided proapoptotic NWs exerted strong anti-glioma activity in two models of GBM, including doubling the lifespan of the mice in an aggressive orthotopic stem cell-like GBM that recapitulates the histological hallmarks of human GBM. Our study suggests that LinTT1 targeting strategy can be used to increase GBM uptake of systemic nanoparticles for improved imaging and therapy.

1. Introduction

Glioblastoma (GBM), the most aggressive form of primary brain cancer, is diagnosed in over 20,000 people in the EU annually [1]. The grim reputation of GBM is due to poor efficacy of standard treatment protocols, which consist of an aggressive regimen comprising surgery, followed by adjuvant therapy in the form of radiation therapy and/or chemotherapy [2]. Despite serious side effects, such treatments result in only marginal improvement in median overall and 5-year survival rates (15 months and 3–5%, respectively). An important cause for failure of the therapies lies within the chemotherapy component of the regimen, as the standard chemotherapeutic of GBM, temozolomide, has a modest anti-cancer effect, is inefficient in accumulating and penetrating the brain tumor lesions and is prone to therapeutic escape due to upregulation of O6-methylguanine-DNA-methyltransferase (MGMT), which counteracts temozolomide-induced DNA alkylation [3]. In contrast to the GBM core that is rich in newly formed leaky vessels and relatively systemically accessible, the infiltrating tumor cells are supplied by vessels with intact blood-brain-barrier (BBB) properties and therefore poorly accessible for systemic imaging agents and drugs [4].

* Corresponding author at: Laboratory of Cancer Biology, Institute of Biomedicine, Centre of Excellence for Translational Medicine, University of Tartu, Tartu, Estonia.
** Correspondence to: Friedmann-Morvinski, Sagol School of Neuroscience, Department of Biochemistry and Molecular Biology, The George S. Wise Faculty of Life Sciences, Tel Aviv University, Israel.
E-mail addresses: dino@tauex.tau.ac.il (D. Friedmann-Morvinski), tambet.teesalu@ut.ee (T. Teesalu).
[1] Equal contribution

https://doi.org/10.1016/j.jconrel.2019.06.018
Received 15 February 2019; Received in revised form 14 June 2019; Accepted 16 June 2019
Available online 27 June 2019

Precision-guided delivery of anticancer compounds with affinity ligands (such as peptides or antibodies) can be used to achieve outcomes similar to topical application: an increased concentration of the drug at the intended target site and a lower exposure in non-target organs. Homing peptides have several advantages over antibodies as affinity targeting ligands: peptides retain the target specificity of antibodies while being easier and cheaper to manufacture, due to their lower affinity, peptides are not subject to the binding site barrier that limits the target distribution of high-affinity antibodies, and they are less immunogenic. Over the years a number of tumor homing peptides have been identified and preclinically developed for targeted drug delivery to solid tumors [5].

TT1 is a tumor homing peptide identified by T7 peptide bacteriophage biopanning on recombinant human p32 (also known as gC1qR) [6]. This protein is a tumor marker because while p32 is located intracellularly (mostly mitochondrially) in quiescent cells, in activated cells it is upregulated and also expressed it at the cell surface, which makes it available for targeting ligands [7,8]. In mitochondria, p32 supports the expression of mitochondrially encoded OXPHOS proteins [9,10]; the role of the cell-surface form of p32 is not known. In the context of tumor affinity targeting, p32 was first identified as the binding partner for the LyP-1 homing peptide which targets tumor lymphatics, tumor macrophages, and malignant cells [11–13]. Compared to normal tissues, in solid tumors, p32 is overexpressed, often in hypoxic areas deep in the tumor parenchyma [13]. TT1 and its linear form (LinTT1, AKRGARSTA) bind p32 with higher affinity than LyP-1 peptide and belong to a class of tumor homing peptides known as tumor-penetrating peptides [6]. These peptides use a multistep pathway for tumor accumulation and penetration [14,15]: upon recruitment of to their cell-surface receptor (p32 in the case of the cyclic and linear TT1 peptides, and LyP-1), tumor-penetrating peptides are proteolytically processed to C-terminally expose a C-end Rule motif RXXR/K-OH (RGAR-OH in TT1), which binds to another receptor, neuropilin-1 (NRP-1). The NRP-1 binding activates a cascade of endocytic/exocytic transcytosis, extravasation and tumor penetration [16–20]. Iron oxide nanoworms (NWs) coated with LinTT1, a nanocarrier system optimized for peptide-mediated tumor targeting [21–25], home efficiently to solid tumors, and systemic administration of NWs coated with a chimeric peptide composed of LinTT1 in tandem with apoptotic $_{D}$(KLAKLAK)$_2$ peptide inhibits progression of aggressive preclinical breast tumors [17] and peritoneal carcinomatosis [25].

Here we studied the effect of LinTT1 functionalization on the tumor homing and therapeutic efficacy of NWs in 5 different GBM xenograft models in mice. Our data show that LinTT1-guided nanoparticles, upon systemic administration, homed to the tumors in all tested GBM models independent of the angiogenic/invasive status of the tumor, and that LinTT1 targeting can be used to potentiate anti-GBM activity of therapeutic nanoparticles.

2. Materials and methods

2.1. Peptides and NW preparation

Peptides were synthesized using Fmoc/t-Bu chemistry using microwave-assisted automated peptide synthesizer (Liberty, CEM Corporation, NC, USA), purified by HPLC using 0.1% TFA in acetonitrile-water mixture to 90%–95% purity and validated by Q-TOF mass spectral analysis. Fluorescent peptides with blocked C-terminus were synthesized in-house by using 5(6)-carboxyfluorescein (FAM) with 6-aminohexanoic acid spacer attached to the N-terminus of the peptide, or ordered from a commercial supplier (TAG Copenhagen, Denmark).

Peptide-functionalized NWs were prepared as previously described [27,28]. Briefly, aminated NWs were PEGylated with maleimide-5KPEG-NHS (JenKem Technology, TX, USA). Peptides were coupled to NWs through a thioether bond between the thiol group of a cysteine residue added to the N-terminus of the peptide and the maleimide on the functionalized particles. Dynamic Light Scattering (DLS; Zetasizer Nano ZS, Malvern Instruments, UK) was used to determine the polydispersity and size of NW preparations. Transmission electron microscopy (TEM; Tecnai 10, Philips, Netherlands) was used to image the nanoparticles.

2.2. Isotopic AgNP synthesis and functionalization

Isotopically-barcoded AgNP were synthesized using a modified Lee and Meisel citrate method [29,30]. Isotopically pure (^{107}Ag or ^{109}Ag) $AgNO_3$ (50.4 mg) was dissolved in the dark in 1 ml of Milli-Q water (MQ, resistivity 18 MΩ cm) and added to 500 ml of water heated at 65 °C in a glass flask cleaned with Piranha solution (H_2SO_4 and H_2O_2; *Caution*: highly oxidizing acid solution). Tannic acid (1.2 mg) was dissolved in 10 ml of MQ and 200 mg of citrate tribasic dihydrate was added to the solution. This mixture was added to the $AgNO_3$ solution in the reaction vessel. The mixture was vigorously stirred at ~ 70 °C and the reaction was allowed to proceed for 3 min, at which point the solution turned yellow. The flask was then transferred to a pre-heated hotplate, boiled for 20 min, and left to cool down to RT. The boiled-off volume was reconstituted with fresh MQ.

The particles were functionalized with NeutrAvidin (NA) to allow conjugation with biotinylated-peptides and lipoic acid-polyethylene glycol(1 k)-NH2 (PEG) as previously described [31]. The terminal amines of PEG were used for coupling of CF555-N-hydroxysuccinimide-dye (NHS-dye). Biotin-X-LinTT1-OH (X, aminohexanoic acid) peptide was coated on ^{109}Ag NPs, and ^{107}Ag NPs were blocked with free D-biotin. The AgNPs were washed to remove free peptides by centrifugation at 7000G, decanting, and resuspension in fresh buffer (0.1 M HEPES pH 7.2, 0.1 M $NaNO_3$, 0.005% Tween-20) with sonication.

2.3. Coupling of LinTT1 to albumin-paclitaxel nanoparticles

For peptide coupling, 5 mg of Abraxane (Celgene) was dissolved in 1 mL of PBS (previously purged with nitrogen) and combined with 0.3 mg (0.6 μmols) of linker sulfosuccinimidyl 4-(*N*-maleimidomethyl) cyclohexane-1-carboxylate in 0.2 mL of PBS. The mixture was stirred for 30 min at RT and Abraxane was purified using a NAP-10 column (GE Healthcare Life Sciences). 0.25 μmol of LinTT1 peptide with N-terminal extra cysteine residue dissolved in 0.2 mL of PBS was slowly added to the purified Abraxane product, the mixture was stirred for 1 h at RT and purified by gel permeation chromatography using Sepharose 4B columns (GE Healthcare Life Sciences).

2.4. Cells and animals

U87-MG GBM cells were obtained from ATCC, and NCH421K cells from CLS Cell Lines Service GmbH (Eppelheim, Germany). WT-GBM and VEGF-KO GBM cells were a gift from Gabriele Bergers (Leuven, Belgium), and 005 cells were established from murine GBM as previously described in [32].

Cell culture reagents were from Gibco (USA) if not stated otherwise. WT-GBM and VEGF-KO-GBM cell lines [32] were cultured in MEM with Earl's salts (Capricorn Scientific, Germany) supplemented with 100 IU/ml of penicillin/streptomycin, 1% sodium pyruvate, 0.01 M HEPES, 0.6% glucose (Applichem, USA) and 5% of heat-inactivated fetal bovine serum (GE Healthcare, UK). NCH421k cells [33] were cultivated in neurobasal medium complemented with B27 neurobasal supplement (Thermo Fisher Scientific, USA), 100 IU/mL of penicillin/streptomycin, 0.4 mM Glutamax, 20 ng/ml basic FGF, 20 ng/ml EGF and 40 μg/ml of heparin (Sigma-Aldrich, USA). U87-MG cells (ATCC HTB14) were grown in DMEM (Lonza, Belgium) containing 100 IU/mL of penicillin, streptomycin, 10% of heat-inactivated fetal bovine serum, 1% sodium pyruvate and 1% non-essential amino acids (Sigma-Aldrich, USA). All cells were cultured at 37 °C in a humidified atmosphere containing 5% CO_2.

Athymic nude mice were purchased from Envigo (The Netherlands). Female mice were used in all *in vivo* experiments if not stated otherwise. For induction of orthotopic GBM xenografts in nude mice, 7×10^5 (WT-GBM, VEGF-KO-GBM) or 3×10^5 (NCH421k) cells were implanted intracranially in the right striatum of the brain (coordinates: 2 mm laterally and 2 mm posteriorly from bregma and at 2.5 mm depth). For induction of s.c. U87-MG tumors, 4×10^6 cells were injected under the skin of the right flank of nude mice. Intracranial tumors were allowed to develop for 6–7 (WT-GBM), 12–14 (VEGF-KO-GBM), or ~30 (NCH421k) days before performing experiments. U87-MG s.c. tumors were allowed to grow until tumors had reached ~ 1 cm^3. Animal experimentation protocols were approved by Committee of Animal Experimentation of Estonian Ministry of Agriculture (Permit #48) and by the Tel Aviv University Institutional Animal Care and Use Committee.

2.5. Evaluation of cellular uptake of nanoworms

For flow cytometry, 3×10^5 WT-GBM, VEGF-KO-GBM, NCH421k, or U87-MG cells in suspension were slowly rotated at 37 °C in the presence of 30 μg/ml NWs in PBS supplemented with 1% BSA (PBS/PSA) for 1 h. After incubation, the cells were washed twice with PBS/BSA, and analyzed by flow cytometry (Accuri, BD Biosciences, USA). The effect of anti-p32 antibody inhibition on LinTT1-NW internalization was studied by pre-incubating the cells in suspension at 37 °C with 20 μg/ml of in-house affinity-purified rabbit polyclonal p32 antibody for 1 h, followed by NW incubation at 37 °C for 1 h, washes at RT, and flow cytometry.

2.6. In vivo biodistribution studies

FAM-labeled NWs were injected intravenously (7.5 mg/kg Fe), and 1 or 5 h later the animals were perfused with 20 mL of DMEM supplemented with 1% BSA. The organs were excised, imaged under Illumatool MMB-MAT (Lightool Research, USA) with 520 nm band-pass filter, snap-frozen in liquid nitrogen, and stored at − 80 °C. For confocal microscopy, the tissues were sectioned at 10 μm and stained with antibodies and DAPI.

To assess the *in vivo* homing of the p32 antibody, 200 μl of affinity-purified rabbit polyclonal anti-p32 antibody in PBS was injected intravenously to mice bearing intracranial WT-GBM or s.c. U87-MG tumors. After 20 min circulation the animals were perfused with PBS through the left ventricle of the heart, the tissues were snap-frozen in liquid nitrogen, and cryosectioned in slices of 10 μm thickness. Tissue sections were stained with 1:1000 goat anti-rabbit Alexa 546 antibody and visualized by confocal microscopy using Olympus FV1200MPE system (Olympus, Germany).

For *in vivo* homing of isotopically barcoded AgNPs, the ^{107}Ag and ^{109}Ag particles were suspended at equimolar ratio in 200 μl PBS (absorbance of biotin-^{107}Ag and LinTT1-^{109}Ag solutions at 400 nm were 11.1 and 5.8, respectively) and injected into tail vein of U87-MG s.c. tumor-bearing athymic nude mice. After 5 h circulation, the mice were perfused *via* the left ventricle of the heart with 20 mL PBS. Organs were divided in two (to obtain material for both extract- and tissue section-based ICP-MS), and snap-frozen in liquid N_2.

2.7. Tissue immunofluorescence and confocal microscopy

Cryosections (10 μm) on Superfrost Plus slides were equilibrated at RT, fixed in cold methanol, washed in PBS and blocked in PBS containing 0.05% Tween-20, 5% FBS, 5% BSA, and 5% goat serum (GE Healthcare, UK) for 1 h. The sections were immunostained with rabbit anti-fluorescein (cat #A889, Thermo Fisher Scientific, MA, USA), rat anti-mouse CD31 (cat #553371, BD Pharmingen, USA), rat anti-mouse CD68 (cat #MCA1957GA, AbD Serotec, USA), rat anti-mouse CD206 (cat #MCA2235GA, Bio-Rad, USA), rat anti-mouse LYVE-1 (cat #14–0443, Affymetrix, USA), and rabbit anti-cleaved caspase-3 (cat #966, Cell Signaling Technology, USA) as primary antibodies. Alexa 488-conjugated goat anti-rabbit IgG, Alexa 647-conjugated goat anti-rat IgG, Alexa 546-conjugated goat anti-rabbit IgG (all Invitrogen, Thermo Fisher Scientific, USA) were used as secondary antibodies. To detect endogenous IgG as a marker of blood vessel leakiness, we stained to tissue sections with Alexa 546 goat anti-mouse IgG, (#Cat.No: A11003; Invitrogen, Thermo Fisher Scientific, USA) at 1/400 dilution. Nuclei were counterstained with 1 μg/ml DAPI. The tissue sections were examined by Olympus FV1200MPE confocal microscope (Olympus, Germany), and the images were processed and analyzed using the FV10-ASW 4.2 Viewer image software (Olympus, Germany) and Image J freeware.

2.8. Experimental tumor therapy

For experimental therapy of mice bearing s.c. U87-MG tumors, 1×10^6 cells were injected under the skin of dorsal flank of 11–15-week old male nude mice. Tumor volume [calculated with the formula: V = (width × width × length)/2] and mouse weight was recorded every other day. When tumors reached 100–200 mm^3 in size, the mice were divided in 4 groups ($n = 6$) so that the total volume of tumors in all groups were equal. Treatment with intravenous FAM-LinTT1-NW, FAM-$_D$(KLAKLAK)$_2$-NW, or FAM-LinTT1- $_D$(KLAKLAK)$_2$-NWs (at 5 mg/kg Fe per injection), or 100 μl of PBS, was started on day 36 after tumor induction. Eight injections in total were performed on every other day. The study was terminated when the first tumor reached 1.5 cm^3. Mice were sacrificed by perfusion and tissues were snap-frozen for further analysis.

For experimental therapy of mice bearing orthotopic syngeneic 005 tumors, 3×10^5 cells were injected in the hippocampus (coordinates: 1.5 mm laterally and 2 mm posteriorly from bregma and at 2.3 mm depth) of 8–12 weeks old C57BL/6 female mice. Ten days after transplantation of tumor cells, mice were divided in 5 groups ($n = 6$) and treated intravenously with either FAM-NW, FAM-LinTT1-NW, FAM-$_D$(KLAKLAK)$_2$-NW, or FAM-LinTT1- $_D$(KLAKLAK)$_2$-NWs (at 5 mg/kg Fe per injection), or 100 μl of PBS. Mice were treated for 2 weeks, 7 injections in total performed on every other day. Mice showing symptoms of disease were sacrificed and tissues collected for further analysis.

2.9. Laser ablation ICP-MS

For ratiometric laser ablation (LA) ICP-MS-based biodistribution studies, the organs from mice injected with Ag-NPs were collected, snap-frozen, cryosectioned in slices of 30 μm thickness on Superfrost Plus slides and air-dried. Determination of $^{109}Ag/^{107}Ag$ ratio in tissue sections was performed using Cetac LSX-213 G2 + laser ablation system (Teledyne Cetac Technologies, USA) using a HelEx 2-volume ablation cell on Agilent 8800 ICP-MS system. The LA-ICP-MS setup was optimized using NIST 612 glass slides. The same reference sample was used to monitor the ThO/Th ratio during the analytical run, which remained under 0.3%. The experimental parameters for the LA system are presented in Supplementary Table 1. ^{13}C, ^{107}Ag and ^{109}Ag isotopes were monitored with dwell times of 47.5 ms, 95 ms and 95 ms respectively, corresponding to a duty cycle of 0.25 s. ^{13}C was used as internal standard to account for differences in the carbon content of the ablated tissue.

2.10. Statistical analysis

For quantification of FAM signal in tissue sections, fluorescence signal intensity of antibody-amplified FAM from 6 to 9 confocal images was quantified using Image J freeware. Co-localization analysis between LinTT1-NW and cellular markers was performed by FV10-ASW 4.2 Viewer image software (Olympus, Germany). To assess statistical significance, Student's *t*-test was performed either by using GraphPad

Prism Software (Graphpad, CA, USA), or one-way analysis of variance (ANOVA). For evaluation of statistical significance of results of the treatment studies, two-way ANOVA Bonferroni's multiple comparison test was used. * – $p \leq .05$, ** – $p \leq .01$.

3. Results

3.1. p32 is upregulated across mouse GBM models representing multiple phenotypes

To assess the relevance of p32 axis for GBM targeting, we first studied the distribution of total and systemically accessible p32 in a panel of five GBM models that represent different invasive/angiogenic GBM phenotypes. WT-GBM cells are genetically engineered mouse embryonic astrocytes immortalized with SV-40 large T antigen and transformed by H-Ras; VEGF-KO-GBM sub-line includes additional VEGF gene inactivation. Upon orthotopic implantation in immunodeficient mice, the WT-GBM cells give rise to angiogenic GBM and the VEGF-KO-GBM cells give rise to infiltrative GBM, with clinical symptoms manifesting on days ~7 and ~14, respectively [33]. The 005 GBM model that we used was derived from GBM tumors induced by lentivirus transduction of Cre target sequence (loxP)-dependent activated H-Ras and Akt, and GFP into GFAP-Cre:Tp53+/− on immunocompetent C57BL/6 mice [32]. We also used two models of GBM of human origin: orthotopic NCH421k, an orthotopic stem cell-like GBM of intermediate phenotype [34], and s.c. U87-MG "classic" model [35]. In the past we have detected robust upregulation of p32 immunoreactivity in the 005 GBM sections compared to the normal brain [36]. Here we first mapped p32 expression status in GBM lesions in other models in our panel (Fig. S1A). In orthotopic WT-GBM and NCH421k, the p32 immunoreactivity was upregulated in the bulk of the tumor and in the malignant foci and thread-like structures projecting away from it (Fig. S1A). In the VEGF-KO-GBM non-angiogenic model that grows by co-opting the brain microvessels, perivascular tumor islets showed strong positivity for p32 expression. In the U87-MG s.c. GBM, p32 immunoreactivity was more prominent at tumor rim with weaker signal deeper in the tumor tissue (Fig. S1A). To map systemically accessible p32, we studied the biodistribution of i.v.-administered rabbit polyclonal anti-p32 antibody. In mice bearing WT-GBM, the accumulation pattern of systemic p32 antibody paralleled the staining of the tumor sections with anti-p32 antibody, with immunoreactivity observed in the tumor periphery with sparse stained cells present inside the tumor bulk (Fig. S1B). In U87-MG tumors, the i.v. p32 antibody was predominantly seen at the areas of lower cellular density at the rim of the tumor (Fig. S1B). In addition, the GBM lesions of models in our panel were positive for NRP1, the receptor of processed linTT1 (Fig. S2).

The status of the vascular barrier has a profound effect on the GBM drug delivery of therapeutic and imaging compounds. Vascular barrier in 005 and U87MG tumors is reported to be compromised [37–39]. To assess the status of the blood brain barrier in the orthotopic NCH421k, WT-GBM, and VEGF-KO-GBM models we immunostained the sections of tumors from perfused mice for the presence of endogenous immunoglobulins (Fig. S3). Whereas microvessels in the normal brain showed no IgG signal, intracranial NCH421k and WT-GBM lesions showed abundant perivascular IgG in line with compromised microvascular BBB (Fig. S3A,B). In contrast, VEGF-KO GBM that relies primarily on co-opted blood vessels for nutrient supply [33] showed lower perivascular immunoglobulin deposits, suggesting a mild BBB impairment (Fig. S3C).

These studies showed the presence of upregulated total and systemically accessible p32 in the GBM models in our panel and suggested that p32-targeted homing peptides can be used for precision targeting of brain tumors.

3.2. Systemic LinTT1-iron oxide nanoworms home to GBM lesions

For affinity targeting of p32, we decided to use LinTT1 peptide, a recently identified ligand of p32 that has been used for *in vivo* targeting of nanoparticles to triple-negative breast cancer [17,40] and peritoneal carcinomatosis [26]. We prepared LinTT1 iron oxide nanoparticles that are due to their high aspect ratio termed nanoworms (NWs), as described previously [21,22]. FAM-LinTT1, or FAM alone were coupled to the NWs through a thioether bond between the cysteine thiol from the peptide or FAM and maleimide groups on the particles, resulting in peptide (or FAM) loading of ~165 μmol/g of iron. In TEM, the NWs appeared as ~100 nm strings of iron cores with ~30 nm diameter (Fig. S4). After LinTT1 coupling, the mean hydrodynamic size of NWs was ~88 nm. Zeta potential was −5.4 +/− 0,2 mV for the "naked" NWs and − 6.9 +/− 0.2 mV for LinTT1 -NWs.

FAM-LinTT1-NWs showed minimal binding to GBM cell lines in culture (Fig. S5) – not a surprising finding given that p32 is predominantly presented on surface tumor stromal cells and under exposure to stress conditions (*e.g.* hypoxia, nutrient deprivation) *in vivo* [13]. Following i.v. administration of FAM-NWs and 5 h circulation, macroscopic *ex vivo* imaging of excised GBM tumors and control organs demonstrated increased presence of FAM-LinTT1-NWs, with WT-GBM showing particularly robust uptake (Fig. S6A). In contrast, GBM lesions from mice injected with control non-targeted NWs showed only a background fluorescence (Fig. S6B). Confocal imaging of FAM fluorescence in sections of these tumors and GFP^+ 005 GBM immunostained with FAM-reactive antibody showed that LinTT1 functionalization increased tumor accumulation of NWs ~3–8 fold (Fig. 1). GFP^+ 005 tumor cells were mostly negative for the uptake for NWs (Fig. S7). Accumulation of LinTT1-NWs in tumor tissue increased over time. In contrast to robust accumulation at 5-h time point, only a weak LinTT1-NW signal in sparse $CD31^+$ structures was detected after 1-h circulation (Fig. S8). LinTT1-coating increased NW accumulation only in the malignant tissue; both LinTT1-NWs and control NWs were found at similar levels in control organs, including the brain (Fig. S9). These data show that LinTT1 functionalization improves tumor homing of NWs across a panel of phenotypically diverse preclinical GBMs.

3.3. LinTT1-NWs co-localize with tumor macrophages and endothelial cells

LyP-1, the first peptide used for systemic targeting of p32, homes to tumor macrophages, as well as blood and lymphatic endothelial cells [11,12]. To establish cellular tropism for LinTT1-NWs in GBM, we stained tumor sections of GBM mice injected with FAM-LinTT1-NWs with cell type-specific marker antibodies against CD31 (blood vessels), CD68 (total macrophages), CD206 (M2-skewed macrophages),

3.4. LinTT1 directs systemic Abraxane and silver nanoparticles to GBM

The structural and physicochemical properties of nanocarrier platform can have a profound effect on biodistribution and targetability with affinity ligands [41]. To determine whether LinTT1 affinity targeting of GBM is compatible with the precision delivery of nanocarriers other than NWs we studied the effect of LinTT1 functionalization on the GBM homing of two additional types of nanoparticles: Abraxane (nanoformulated paclitaxel-albumin; Nab-paclitaxel) and metallic silver nanoparticles. First, we injected WT-GBM mice i.v. with 0.5 mg of LinTT1-FAM-Abraxane, or FAM-Abraxane without the peptide. After 5 h of circulation, FAM-LinTT1-Abraxane signal was found in tumor blood vessels and in scattered cells in tumor parenchyma, whereas non-targeted FAM-Abraxane showed no detectable GBM accumulation (Fig. S14A, C).

We next tested the effect of LinTT1 functionalization on the tumor homing of silver nanoparticles. Two types of AgNPs were used: isotopically pure ^{109}AgNPs coated with biotinylated LinTT1 peptide and non-targeted biotin ^{107}AgNPs. Mice bearing s.c. U87-MG tumors were

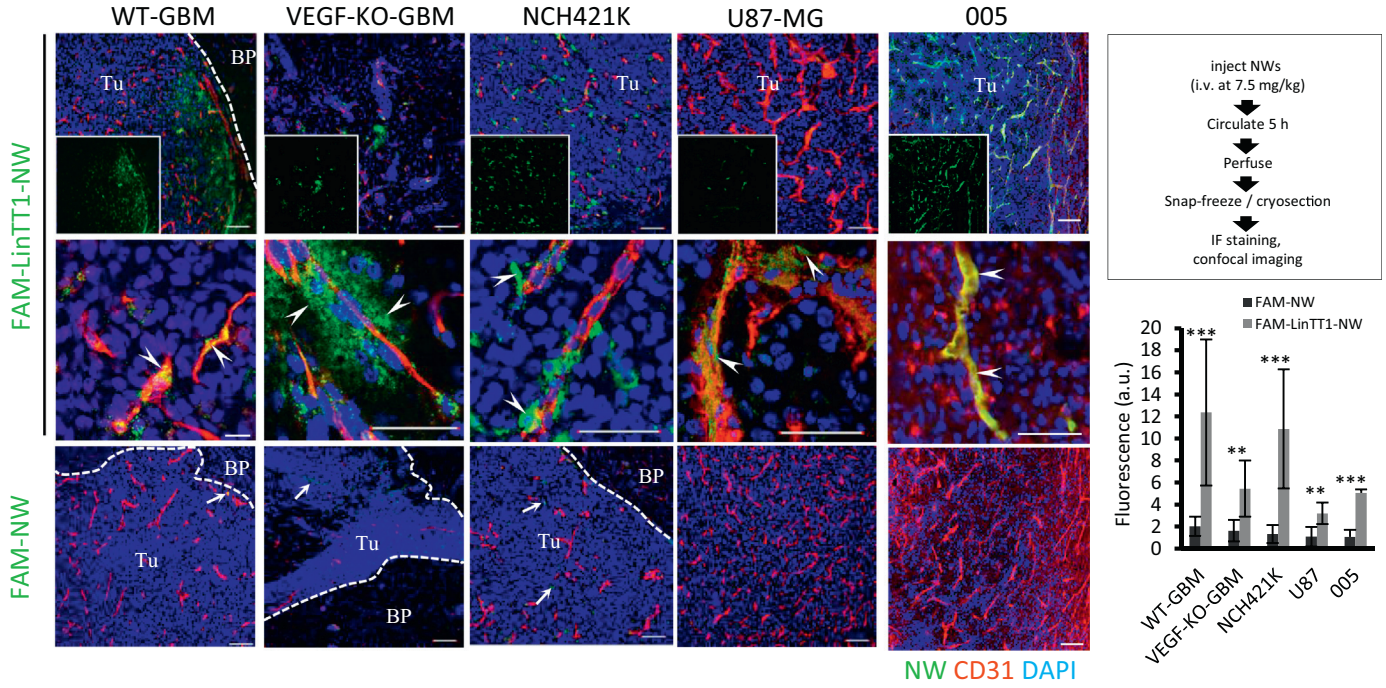

Fig. 1. FAM-LinTT1-iron oxide nanoworms home to mouse and human GBM. Mice bearing GBM xenografts of mouse (005, WT-GBM, VEGF-KO-GBM – intracranial) or of human origin (NCH421k – intracranial, U87-MG – subcutaneous) were injected intravenously with 7.5 mg/kg FAM-LinTT1-NW or FAM-NW, and allowed to circulate for 5 h followed by cardiac perfusion of the animals. Cryosections from subcutaneous tumor or coronal cryosections from brain with GBM were stained by anti-FAM (NWs), anti-CD31 (blood vessels), and DAPI (cell nuclei) and visualized by confocal microscopy. Tu – tumor, BP – brain parenchyma. Insets show the FAM channel alone. Arrowheads indicate LinTT1-NW signal. Scale bars – 100 μm in low magnification panels; 50 μm in high magnification panel. FAM-LinTT1-NW and FAM-NW signal intensity in GBM tissue was quantified from 6 to 9 confocal images and analyzed by Image J. Statistical analysis was performed by one-way ANOVA. Error bars: standard deviation.

injected i.v. with an equimolar mixture of LinTT1-^{109}AgNP and control-^{107}AgNP, and after 5 h, perfused to remove free background particles. The ratio of the targeted to untargeted AgNPs in tumor and control tissues was analyzed by laser ablation ICP-MS, a technique that allows spatial ratiometric analysis of $^{109/107}$AgNPs in tissue sections [42]. Tumor sections showed the presence of peaks in the $^{109/107}$AgNP ratio ($^{109/107}$Ag range: ~5–30) in line with preferential tumor homing of LinTT1-^{109}Ag particles (Fig. S14B). Correlative analysis of the LA-ICP-MS profiles with morphological landmarks along the laser ablation paths indicated that elevated ratios of $^{109}/^{107}$Ag were predominantly seen in the tumor areas rich in tumor vessels. In contrast, the $^{109/107}$Ag ratio in the liver was uniform at ~1.5 (Fig. S14D), providing a baseline ratiometric estimate (Fig. S14D). These experiments show that LinTT1 functionalization increases *in vivo* the GBM accumulation of nanoparticles of different classes.

3.5. Proapoptotic LinTT1- NWs inhibit GBM growth

Finally, we evaluated the effect of LinTT1 conjugation on the anti-GBM activity of NWs loaded with a therapeutic payload, amphiphilic proapoptotic $_D$(KLAKLAK)$_2$ peptide. This peptide has been used as a payload in numerous therapeutic studies with NWs [24,26]. $_D$(KLAKLAK)$_2$ peptide exerts its apoptotic effect through the destabilization of the mitochondrial membrane, and we have reported that the LinTT1-NWs are intracellularly routed to mitochondria in cells expressing cell-surface p32 [26].

We first tested the effect of LinTT1-targeted proapoptotic NWs on U87-MG s.c. tumor which allowed us to monitor tumor size, rather than using survival as the endpoint. The daily injected dose and cumulative dose of NWs were chosen based on the study by Agemy et al. (2011), in which the CGKRK-D(KLAKLAK)2-NWs were found to have a robust anti-GBM activity and moderate side effects (mild reversible hepatotoxicity) [24]. In agreement with good tolerability, we did not observe weight loss in any treatment group (Fig. S16). We found that the tumor mice treated with LinTT1-$_D$(KLAKLAK)$_2$-NWs showed slower progression of tumor growth than controls, starting already after the 2nd injection of LinTT1-$_D$(KLAKLAK)$_2$-NWs on day 40 post tumor induction (Fig. S15), and tumor size at the end of the treatment was significantly reduced ($p < .01$) compared to the PBS group. The other treatments, including $_D$(KLAKLAK)$_2$-NW, did not significantly affect tumor growth.

Encouraged by this GBM treatment study, we decided to assess the preclinical efficacy of the LinTT1-guided proapoptotic nanosystem in the orthotopic 005 GBM, which expresses stem cell markers and recapitulates the histological hallmarks of human GBM. Experimental therapy of 005 GBM was initiated 10 days after transplantation of the tumor cells (~1/3 of the latency of the tumors), which corresponds to tumor volume of approximately 0.8–1.0 mm^3 (as assessed by volumetric microscopy). In the experimental glioma treatment literature, tumors of this size are considered well established [43]. Compared to control groups, the LinTT1-$_D$(KLAKLAK)$_2$-NW treatment group showed greatly improved survival (Fig. 3B). When body weight loss (Fig. S17) and impaired motor functions of mice in the PBS group necessitated sacrifice of these mice, the LinTT1- $_D$(KLAKLAK)$_2$-NW-treated group did not show impaired health, suggesting suppressed tumor growth. The small size of the tumor in one mouse sacrificed from this group agreed with this notion (Fig. 3C). Fluorescent lectin injections and von Willebrand factor staining at sacrifice revealed almost complete absence of patent blood vessels and endothelial cells in the tumors treated with the LinTT1- $_D$(KLAKLAK)$_2$-NWs, whereas the control tumors were well vascularized (Fig. 4A, B and Fig. S18). In agreement with their slow growth, very few Ki67-positive proliferating cells were detected in the LinTT1- $_D$(KLAKLAK)$_2$-NW tumors (Fig. 4C). These therapy studies indicate that LinTT1 targeting may be used to potentiate the activity of anticancer nanoparticles.

Representative images from 3 independent experiments are shown. Scale bar = 50 μm.

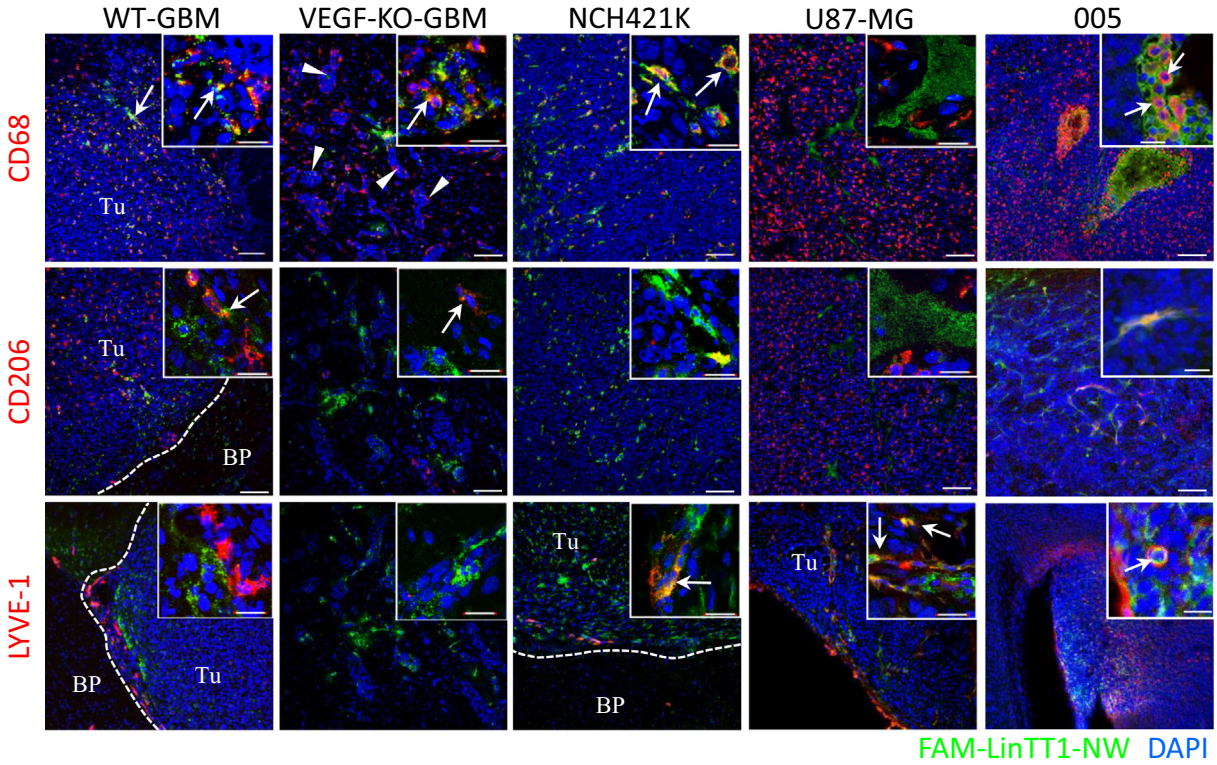

Fig. 2. Cellular distribution of FAM-LinTT1-NWs in GBM lesions. Mice bearing GBM models of mouse origin (005, WT-GBM, VEGF-KO-GBM – intracranial) and of human origin (NCH421k – intracranial, U87-MG – subcutaneous) were injected intravenously with 7.5 mg/kg FAM-LinTT1-NW, or FAM-NW, and allowed to circulate for 5 h followed by cardiac perfusion of the animals. (A) – Cryosections of subcutaneous U87-MG tumor or coronal cryosections from orthotopic GBMs were stained the following antibodies: anti-FAM (nanoworms), anti-CD68 (pan-macrophage marker), anti-CD206 (M2 macrophage marker), anti-LYVE-1 (lymphatic vessels); counterstained with DAPI to visualize the cell nuclei, and imaged by confocal microscopy. Scale bar on low-magnification image – 100 µm. Scale bar on insets – 20 µm. Tumor nodules in VEGF-KO-GBM are indicated by arrowheads. Arrows indicate colocalization. Tu – tumor, BP – brain parenchyma and LYVE1 (lymphatic vessels). In our GBM panel, NCH421k was negative for the presence of CD206-positive M2 macrophages and VEGF-KO-GBM did not contain detectable LYVE1-positive lymphatic endothelial cells (Fig. 2, Fig. S10), whereas the remaining models contained each of the three cell populations. In the orthotopic GBM, LinTT1-NW signal showed an extensive overlap with CD31 and CD68 immunoreactivities (Figs. 1 and 2, Fig. S10). Despite the presence of numerous CD68-positive cells in s.c. U87-MG GBM, the LinTT1-NWs accumulated predominantly in blood vessel endothelial cells in these tumors. Sparse LYVE-1-positive lymphatic structures in the periphery of WT-GBM, NCH421k and U87-MG tumors took up LinTT1-NWs at a level comparable that seen for $CD31^+$ blood vessels (Fig. 2, Fig. S10), although the contribution of lymphatic Lin TT1-NW homing to the overall tumor accumulation was low. Whereas LYVE-1 also has functions beyond the lymph vascular system, including in vascular endothelial cells, co-staining of tumor sections for LYVE-1 and CD31 showed that in the GBM models used in the current study the Lyve1 and CD31-positive cell populations are mostly distinct (Fig. S11 and 12). In addition to endothelial- and macrophage-associated signals, extravascular LinTT1-NWs in tumor stroma were observed in WT-GBM and VEGF-KO GBM tumors (Fig. 2, arrows). In the 005 tumors, the a LinTT1-NW signal mostly overlapped with CD68 and CD31. Although only a small fraction of the cells in the 005 tumors were CD206 positive, these cells also showed positive overlay with LinTT1-NW signal. Remarkably, in these tumors, a robust uptake of LinTT1-NWs was observed in GFP + endothelial cells transdifferentiated from the tumor cells (Fig. S13). These studies show that in GBM, LinTT1-NWs predominantly home to macrophages and to the blood/lymphatic endothelial cells.

4. Discussion

Intratumoral heterogeneity is a key factor that allows high grade gliomas to evade increasingly sophisticated therapeutic strategies. Clinical GBM lesions contain regions of infiltrative tumor growth into brain parenchyma, as well as areas of angiogenesis and regions of pseudopalisading necrosis [44]. Here we show that targeting with the tumor-penetrating peptide LinTT1 increases tumor accumulation of three types of systemically administered nanoparticles to each of the five phenotypically diverse models of GBM tested. LinTT1-NWs were found to accumulate in stromal cell populations with established roles in tumor progression: endothelial cells (including tumor-derived endothelial cells) and in tumor associated macrophages. The tumor accumulation translated into potentiated anti-GBM activity. These observations suggest potential applications for LinTT-guided imaging, therapeutic, and theranostic nanoparticles in clinical management of GBM.

In our panel of GBM models, a compromised BBB probably facilitated the transition of the LinTT1-NWs into the extravascular tumor parenchyma. Multi-targeting of nanoparticles with different homing ligands is an increasingly popular strategy to improve target selectivity and the crossing of biological barriers, and it is possible that LinTT1 brain tumor homing may be synergistically improved in combination with a BBB crossing peptide, such as LRP-1 binding Angiopep-2 [45]. The LinTT1 nanoparticles primarily accumulated in stroma-derived cell populations, whereas the tumor cells did not contain detectable nanoparticles. However, given that tumor cells, especially in late tumors, are often found to express the LinTT1 receptor, cell surface p32, the low-level accumulation of the nanoparticles in the tumor cells is possible, and even likely. In addition to uptake in blood vessel and lymphatic endothelial cells, robust accumulation of LinTT1-guided nanoparticles was detected in tumor-associated macrophages, including M2-skewed CD206 + macrophages - a key cell population supporting tumor maintenance, progression, and drug resistance [46]. Elevated M2-like TAMs are found in tumor stroma across a variety of human malignancies [47,48]and targeting these cells may provide novel treatment options to cancer types currently unresponsive to conventional chemotherapies and immunotherapies. Thus, LinTT1 can be used to develop “smart” molecular and nanoscale therapeutic and/or immunotherapeutic agents for selective elimination or reprogramming of

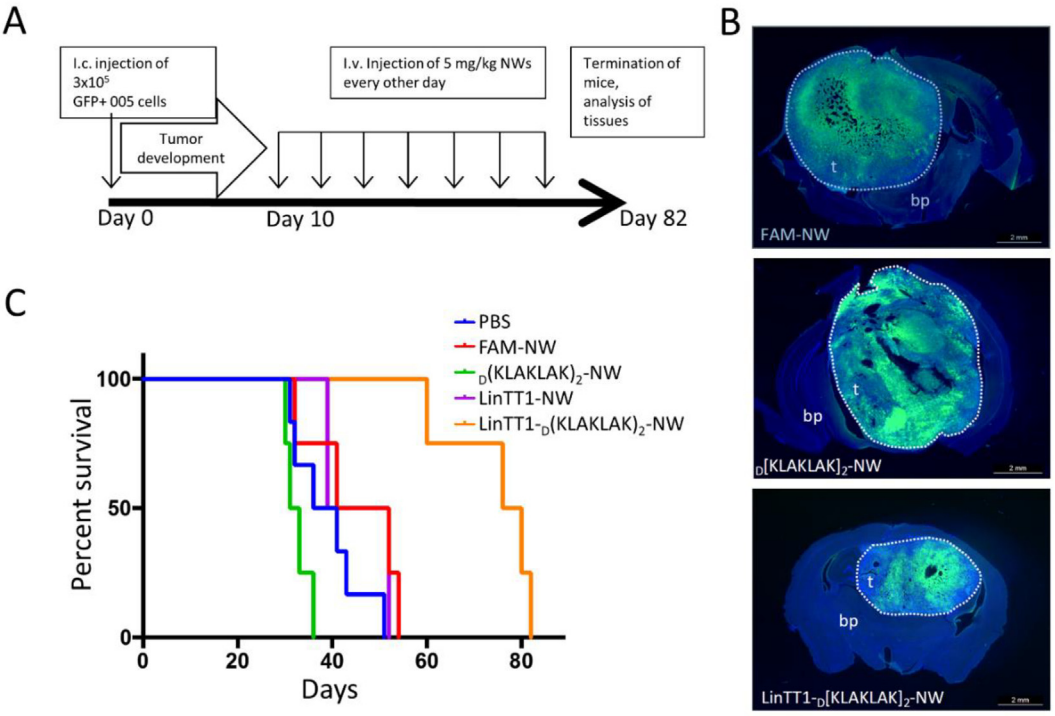

Fig. 3. Experimental therapy of 005 GBM with LinTT1-$_D$(KLAKLAK)$_2$-NW inhibits tumor growth. (A) – Starting on day 10 post tumor induction, the 005-bearing mice received 7 i.v. injections of 5 mg/kg of LinTT1-$_D$(KLAKLAK)$_2$-NW, or control compounds [FAM-$_D$(KLAKLAK)$_2$-NW, FAM-LinTT1- $_D$(KLAKLAK)$_2$-NWs, and PBS] every other day. (B) – Representative images of DAPI -counterstained (blue) sections of orthotopic GBM 005 GBM (GFP positive tumor indicated by dotted line) were collected on day 82 42, 35, and 36 from mice treated with either FAM-NW, FAM-D(KLAKLAK)2-NW and or FAM-LinTT1- D(KLAKLAK)2-NWs, respectively. T: tumor, BP: brain parenchyma. (C) – Body weight and motor functions of mice were monitored daily and the animals were sacrificed when they reached the limits allowed by the animal ethics committee, and the survival data were expressed as Kaplan-Meyer plots. Scale bar = 2 mm. (For interpretation of the references to colour in this figure legend, the reader is referred to the web version of this article.)

TAMs for sustained modulation of tumor microenvironment. Low macrophage uptake of nontargeted NWs reported here and in the past reports [17,24,49] contrasts with promiscuous macrophage uptake of certain nanoparticles, in particular polyglucose nanoparticles consisting of cross-linked dextrans and their derivatives [50]. The “stealthness” of NPs and the extent of their uptake in TAMs is affected by the NP building blocks, chain lengths, cross-linking strategies, particle size, ζ potential, imaging labels, and protein coronas. Blood half life for NWs in mice has been estimated to be in 12–17 h range [22,49] - much longer than the 20 min observed for ~25 nm Feraheme nanoparticles that are robustly taken up by TAMs [51].

Our past studies documented that NWs functionalized with CGKRK, a homing peptide also reported to bind p32, home exclusively to GBM blood vessels [24]. CGKRK is a multireceptor homing peptide that besides p32 interacts with nardilysin [36] and calreticulin [46]. Unlike CGKRK, LinTT1 belongs to a novel class of tumor penetrating peptides – it harbors a cryptic C-end rule (CendR) peptide (RGAR) that upon proteolytic C-terminal exposure acquires the ability to bind to NRP-1, which triggers extravasation and tumor penetration [6,17–19]. The active vascular exit of LinTT1-NWs may be a prerequisite for uptake in tumor associated macrophages and in other cells in the extravascular space. Future studies will address the applicability of LinTT1 targeting (possibly in conjunction with additional macrophage-specific homing peptides such as CD206-targeting UNO peptide [52]), for therapeutic targeting or reprogramming of tumor macrophages.

Solid tumor growth depends on the growth of new vessels and inhibiting angiogenesis has become a mainstream therapeutic anticancer strategy. Interestingly, our studies on the 005 GBM model, where the tumor cells have been engineered to express GFP, showed robust LinTT1-NW uptake in cells that expressed the endothelial differentiation marker CD31 and were GFP-positive. These cells are likely to be tumor-derived cells trans-differentiated into endothelial cells (TDEC). Such cells are known to be generated in the 005 tumors [53]. TDECs are genetically unstable, contain cytogenetic abnormalities, and are prone to resistance to anticancer chemotherapies [53]. TDEC are also clinically relevant; nearly a half of clinical glioblastoma cases contain cells that co-express both GFAP, a marker for astrocytes, the cell of origin of GBM, and a markers for endothelial cells (CD31 and CD34) [54]. TDECs are VEGFR2-negative and nonresponsive to the anti-angiogenic agent bevacizumab (Avastin) [53]. In clinical settings, the TDEC resistance may contribute to the transient effect of Avastin treatment in GBM cases and the frequent increase in tumor aggressiveness seen after anti-angiogenic therapy [55,56]. LinTT1-based delivery strategies may allow targeting blood vessels formed by TDECs.

P32 is prominently expressed in clinical samples and in mouse models of GBM, and there is a significant correlation between high p32 expression and decreased survival of GBM patients [28]. The cell surface p32 expression in brain tumors has been documented in several studies. Agemy et al. established cell-surface expression of p32 by 005 brain tumor cells, T3 brain tumor endothelial cells, and human umbilical vein endothelial cells using flow cytometry [36]. Fogal et al. found that in clinical glioma samples the membrane staining of the p32 antigen was evident [28]. The genetic knockdown of p32 has been demonstrated to limit cell proliferation *in vitro* and tumor growth *in vivo*. p32 targeting ligands possess an intrinsic antitumor activity and pharmacological inhibition of p32 with a low molecular weight compound blocks the proliferation of p32-overexpressing glioma cells, and sensitizes them to glucose depletion [12,57]. It remains to be determined if the intrinsic antitumor effect of peptidic p32 targeting ligands can act in synergy with nanoparticle payload drugs to potentiate the therapeutic efficacy.

Another aspect that requires further studies is the putative

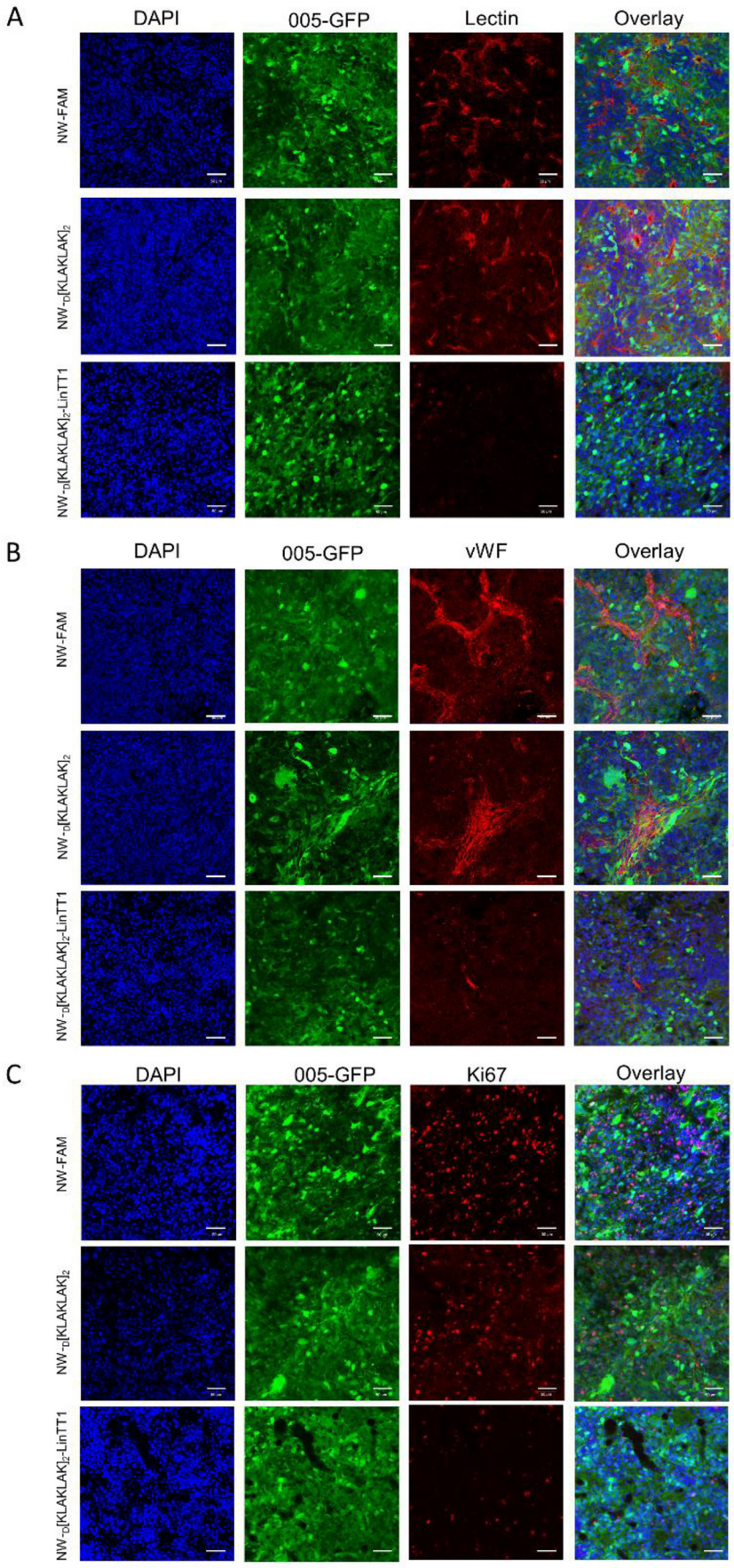

Fig. 4. Experimental therapy of 005 GBM with LinTT1-$_D$(KLAKLAK)$_2$-NW decreases patency of tumor vessels and reduces proliferative activity in tumor tissue. (A) – Treatment of 005 mice with systemic FAM-LinTT1-$_D$(KLAKLAK)$_2$-NWs reduces the density of patent intratumoral blood vessels. 005 mice were i.v. injected with 50 µl 0.1 mg/ml labeled wheat germ agglutinin (WGA) and after 10 min circulation the unbound lectin was removed by perfusion with PBS, and tissue was snap-frozen, sectioned and subjected to confocal imaging. Note robust decrease in WGA-positive (red) vascular structures in tumor tissue (green) from mouse treated with FAM-LinTT1-$_D$(KLAKLAK)$_2$-NWs. (B) – Treatment of 005 mice with systemic FAM-LinTT1-$_D$(KLAKLAK)$_2$-NWs reduces the density of intratumoral vWF-positive blood vessels. Cryosections of post-treatment 005 tumors were sectioned, immunostained for vWF (red) and subjected to confocal imaging. (C) – Therapy of 005 mice with systemic FAM-LinTT1-$_D$(KLAKLAK)$_2$-NWs inhibits proliferation of cells in tumors. Cryosections of post-treatment 005 tumors were sectioned, immunostained for proliferation marker Ki67 (red) and subjected to confocal imaging. (For interpretation of the references to colour in this figure legend, the reader is referred to the web version of this article.)

potentiating role of the LinTT1 peptide on co-administered anti-GBM payloads. In a recent study we observed that LinTT1-NWs increase penetration of co-administered payload [26]. Agemy et al. [24]showed that co-administration of iRGD tumor penetrating peptide potentiated tumor accumulation and therapeutic efficacy of the CGKRK-$_D$(KLKLAK)$_2$-NWs. It remains to be seen, if free LinTT1 peptide has similar bystander activity.

In summary, we have shown that a novel p32 targeting peptide, LinTT1, effectively promotes the targeted accumulation of three types of nanoparticles to tumors across a panel of mouse models of high-grade glioma. The treatment of mice with anticancer LinTT1-guided NPs extends the survival of the tumor mice. Given that elevated expression of p32 is found in clinical GBM, and that the LinTT1 peptide recognizes p32 across species, our study warrants follow-up studies on LinTT1 guided therapies.

Acknowledgements

This work was supported by the European Regional Development Fund Mobilitas Plus postdoctoral fellowship MOBJD11 (to L. Simon-Gracia), the European Regional Development Fund (Project No. 2014-2020.4.01.15-0012), by EMBO Installation grant #2344 (to T. Teesalu), European Research Council grants GBMDDS and GLIOGUIDE from European Regional Development Fund (to T. Teesalu), Wellcome Trust International Fellowship WT095077MA (to T. Teesalu), and Norwegian-Estonian collaboration grant EMP181 (to T. Teesalu). We also acknowledge the support of Estonian Research Council (grant PRG230 to T. Teesalu). The work was also supported by the Israel Science Foundation (ISF 1310/15), Israel Cancer Research Fund (ICRF), Marie Curie Career Integration Grants (CIG) and Cancer Biology Research Center (CBRC) to D. Friedmann-Morvinski.

We thank Martin Kärner for the assistance with histological analysis, professor Kalle Kirsimäe with ICP-MS, and Anne-Mari Anton Willmore for critical reading of the manuscript.

Appendix A. Supplementary data

Supplementary data to this article can be found online at https://doi.org/10.1016/j.jconrel.2019.06.018.

References

[1] E. Crocetti, A. Trama, C. Stiller, A. Caldarella, R. Soffietti, J. Jaal, D.C. Weber, U. Ricardi, J. Slowinski, A. Brandes, N. Zielonk, E. Van Eycken, H. Sundseth, S. Marreaud, R. Audisio, G. Hedelin, G. Launoy, A.V. Guizard, A.M. Bouvier, A.S. Woronoff, A. Buemi, B. Tretarre, M. Colonna, S. Bara, O. Ganry, P. Grosclaude, B. Holleczek, J. Geissler, L. Tryggvadottir, H. Comber, F. Bellù, S. Ferretti, D. Serraino, M. Vercelli, S. Vitarelli, M. Federico, M. Fusco, A. Traina, M. Michiara, A. Giacomin, R. Tumino, L. Mangone, F. Falcini, A. Iannelli, M. Budroni, S. Piffer, T. Intrieri, F. La Rosa, P. Contiero, P. Zambon, P.G. Casali, G. Gatta, A. Gronchi, L. Licitra, M. Ruzza, S. Sowe, R. Capocaccia, R. De Angelis, S. Mallone, A. Tavilla, A.P. Dei Tos, A.A. Brandes, K. England, G. Ursin, O. Visser, R. Otter, S. Siesling, J.M. van der Zwan, J.W.W. Coebergh, H. Schouten, J. Rachtan, S. Gozdz, M. Zwierko, M. Bielska-Lasota, J. Slowinski, A. Miranda, C. Safaei Diba, M. Primic-Zakelj, A. Mateos, I. Izarzugaza, A. Torrella-Ramos, R. Marcos-Gragera, M.J. Sánchez, C. Navarro, E. Ardanaz, J. Galceran, C. Martinez-Garcia, J.M. Melchor, J. Adolfsson, M. Lambe, T.R. Möller, U. Ringborg, G. Jundt, M. Usel, S.M. Ess, A. Bordoni, I. Konzelmann, J.M. Lutz, D.C. Greenberg, J. Wilkinson, M. Roche, J. Verne, D. Meechan, G. Lawrence, M.P. Coleman, J. Mackay, A. Gavin, D.H. Brewster, I. Kunkler, J. Steward, Epidemiology of glial and non-glial brain tumours in Europe, Eur. J. Cancer (2012), https://doi.org/10.1016/j.ejca.2011.12.013.

[2] M. Weller, T. Cloughesy, J.R. Perry, W. Wick, Standards of care for treatment of recurrent glioblastoma-are we there yet? Neuro-Oncology (2013), https://doi.org/10.1093/neuonc/nos273.

[3] M.C. Chamberlain, Temozolomide: therapeutic limitations in the treatment of adult high-grade gliomas, Expert. Rev. Neurother. (2010), https://doi.org/10.1586/ern.10.32.

[4] A. Kiviniemi, M. Gardberg, P. Ek, J. Frantzén, J. Bobacka, H. Minn, Gadolinium retention in gliomas and adjacent normal brain tissue: association with tumor contrast enhancement and linear/macrocyclic agents, Neuroradiology. (2019), https://doi.org/10.1007/s00234-019-02172-6.

[5] E. Ruoslahti, Tumor penetrating peptides for improved drug delivery, Adv. Drug Deliv. Rev. (2017), https://doi.org/10.1016/j.addr.2016.03.008.

[6] L. Paasonen, S. Sharma, G.B. Braun, V.R. Kotamraju, T.D.Y. Chung, Z.G. She, K.N. Sugahara, M. Yliperttula, B. Wu, M. Pellecchia, E. Ruoslahti, T. Teesalu, New p32/gC1qR ligands for targeted tumor drug delivery, ChemBioChem. (2016), https://doi.org/10.1002/cbic.201500564.

[7] E.I. Peerschke, K.B. Reid, B. Ghebrehiwet, Identification of a novel 33-kDa C1q-binding site on human blood platelets, J. Immunol. 152 (12) (1994 Jun) 5896–5901.

[8] B.J. Soltys, D. Kang, R.S. Gupta, Localization of P32 protein (gC1q-R) in mitochondria and at specific extramitochondrial locations in normal tissues., Histochem, Cell Biol. (2000), https://doi.org/10.1007/s004180000191.

[9] V. Fogal, A.D. Richardson, P.P. Karmali, I.E. Scheffler, J.W. Smith, E. Ruoslahti, Mitochondrial p32 protein is a critical regulator of tumor metabolism via maintenance of oxidative phosphorylation, Mol. Cell. Biol. (2010), https://doi.org/10.1128/MCB.01101-09.

[10] M. Yagi, T. Uchiumi, S. Takazaki, B. Okuno, M. Nomura, S.I. Yoshida, T. Kanki, D. Kang, P32/gC1qR is indispensable for fetal development and mitochondrial translation: importance of its RNA-binding ability, Nucleic Acids Res. (2012), https://doi.org/10.1093/nar/gks774.

[11] P. Laakkonen, K. Porkka, J.A. Hoffman, E. Ruoslahti, A tumor-homing peptide with a targeting specificity related to lymphatic vessels, Nat. Med. (2002), https://doi.org/10.1038/nm720.

[12] P. Laakkonen, M.E. Akerman, H. Biliran, M. Yang, F. Ferrer, T. Karpanen, R.M. Hoffman, E. Ruoslahti, Antitumor activity of a homing peptide that targets tumor lymphatics and tumor cells, Proc. Natl. Acad. Sci. 101 (2004) 9381–9386, https://doi.org/10.1073/pnas.0403317101.

[13] V. Fogal, L. Zhang, S. Krajewski, E. Ruoslahti, Mitochondrial/cell-surface protein p32/gC1qR as a molecular target in tumor cells and tumor stroma, Cancer Res. (2008), https://doi.org/10.1158/0008-5472.CAN-07-6752.

[14] T. Teesalu, K.N. Sugahara, E. Ruoslahti, Tumor-penetrating peptides, Front. Oncol. 3 (2013) 216, , https://doi.org/10.3389/fonc.2013.00216.

[15] K.N. Sugahara, T. Teesalu, P.P. Karmali, V.R. Kotamraju, L. Agemy, O.M. Girard, D. Hanahan, R.F. Mattrey, E. Ruoslahti, Tissue-penetrating delivery of compounds and nanoparticles into Tumors, Cancer Cell (2009), https://doi.org/10.1016/j.ccr.2009.10.013.

[16] T. Teesalu, K.N. Sugahara, V.R. Kotamraju, E. Ruoslahti, C-end rule peptides mediate neuropilin-1-dependent cell, vascular, and tissue penetration, Proc. Natl. Acad. Sci. 106 (2009) 16157–16162, https://doi.org/10.1073/pnas.0908201106.

[17] S. Sharma, V.R. Kotamraju, T. Mölder, A. Tobi, T. Teesalu, E. Ruoslahti, Tumor-penetrating Nanosystem strongly suppresses breast tumor growth, Nano Lett. (2017), https://doi.org/10.1021/acs.nanolett.6b03815.

[18] X. Liu, P. Lin, I. Perrett, J. Lin, Y.P. Liao, C.H. Chang, J. Jiang, N. Wu, T. Donahue, Z. Wainberg, A.E. Nel, H. Meng, Tumor-penetrating peptide enhances transcytosis of silicasome-based chemotherapy for pancreatic cancer, J. Clin. Invest. (2017), https://doi.org/10.1172/JCI92284.

[19] Y. Akashi, T. Oda, Y. Ohara, R. Miyamoto, T. Kurokawa, S. Hashimoto, T. Enomoto, K. Yamada, M. Satake, N. Ohkohchi, Anticancer effects of gemcitabine are enhanced by co-administered iRGD peptide in murine pancreatic cancer models that over-expressed neuropilin-1, Br. J. Cancer (2014), https://doi.org/10.1038/bjc.2014.49.

[20] H.B. Pang, G.B. Braun, T. Friman, P. Aza-Blanc, M.E. Ruidiaz, K.N. Sugahara, T. Teesalu, E. Ruoslahti, An endocytosis pathway initiated through neuropilin-1 and regulated by nutrient availability, Nat. Commun. (2014), https://doi.org/10.1038/ncomms5904.

[21] J.H. Park, G. Von Maltzahn, L. Zhang, M.P. Schwartz, E. Ruoslahti, S.N. Bhatia, M.J. Sailor, Magnetic iron oxide nanoworms for tumor targeting and imaging, Adv. Mater. (2008), https://doi.org/10.1002/adma.200800004.

[22] J.H. Park, G. Von Maltzahn, L. Zhang, A.M. Derfus, D. Simberg, T.J. Harris, E. Ruoslahti, S.N. Bhatia, M.J. Sailor, G. Von Maltzahn, D. Simberg, T.J. Harris, Systematic surface engineering of magnetic nanoworms for in vivo tumor targeting, Small. 5 (2009) 694–700, https://doi.org/10.1002/smll.200801789.

[23] J.-H. Park, G. von Maltzahn, M.J. Xu, V. Fogal, V.R. Kotamraju, E. Ruoslahti, S.N. Bhatia, M.J. Sailor, Cooperative nanomaterial system to sensitize, target and treat tumors, Proc. Natl. Acad. Sci. 107 (2010) 981–986, https://doi.org/10.1073/pnas.0909565107.

[24] L. Agemy, D. Friedmann-Morvinski, V.R. Kotamraju, L. Roth, K.N. Sugahara, O.M. Girard, R.F. Mattrey, I.M. Verma, E. Ruoslahti, Targeted nanoparticle enhanced proapoptotic peptide as potential therapy for glioblastoma, Proc. Natl. Acad. Sci. 108 (2011) 17450–17455, https://doi.org/10.1073/pnas.1114518108.

[25] L. Roth, L. Agemy, V.R. Kotamraju, G. Braun, T. Teesalu, K.N. Sugahara, J. Hamzah, E. Ruoslahti, Transtumoral targeting enabled by a novel neuropilin-binding peptide, Oncogene. (2012), https://doi.org/10.1038/onc.2011.537.

[26] H. Hunt, L. Simón-Gracia, A. Tobi, T. Teesalu, V.R. Kotamraju, S. Sharma, K.N. Sugahara, E. Ruoslahti, T. Teesalu, M. Nigul, K.N. Sugahara, Targeting of p32 in peritoneal carcinomatosis with intraperitoneal linTT1 peptide-guided pro-apoptotic nanoparticles, J. Control. Release (2017), https://doi.org/10.1016/j.jconrel.2017.06.005.

[27] D. Miao, M. Jiang, Z. Liu, G. Gu, Q. Hu, T. Kang, Q. Song, L. Yao, W. Li, X. Gao, M. Sun, J. Chen, Co-administration of dual-targeting nanoparticles with penetration enhancement peptide for antiglioblastoma therapy, Mol. Pharm. (2014), https://doi.org/10.1021/mp400189j.

[28] V. Fogal, I. Babic, Y. Chao, S. Pastorino, R. Mukthavaram, P. Jiang, Y.-J. Cho, S.C. Pingle, J.R. Crawford, D.E. Piccioni, S. Kesari, R.C. John, D.E. Piccioni, S. Kesari, R. Mukthavaram, P. Jiang, Y.-J. Cho, S.C. Pingle, J.R. Crawford, D.E. Piccioni, S. Kesari, Mitochondrial p32 is upregulated in Myc expressing brain cancers and mediates glutamine addiction, Oncotarget. 6 (2015) 1157–1170, https://doi.org/10.18632/oncotarget.2708.

[29] P.C. Lee, D. Meisel, Adsorption and surface-enhanced Raman of dyes on silver and gold sols, J. Phys. Chem. (1982), https://doi.org/10.1021/j100214a025.
[30] T. Dadosh, Synthesis of uniform silver nanoparticles with a controllable size, Mater. Lett. (2009), https://doi.org/10.1016/j.matlet.2009.07.042.
[31] G.B. Braun, T. Friman, H.B. Pang, A. Pallaoro, T.H. De Mendoza, A.M.A. Willmore, V.R. Kotamraju, A.P. Mann, Z.G. She, K.N. Sugahara, N.O. Reich, T. Teesalu, E. Ruoslahti, Etchable plasmonic nanoparticle probes to image and quantify cellular internalization, Nat. Mater. (2014), https://doi.org/10.1038/nmat3982.
[32] T. Marumoto, A. Tashiro, D. Friedmann-Morvinski, M. Scadeng, Y. Soda, F.H. Gage, I.M. Verma, Development of a novel mouse glioma model using lentiviral vectors, Nat. Med. (2009), https://doi.org/10.1038/nm.1863.
[33] B. Blouw, H. Song, T. Tihan, J. Bosze, N. Ferrara, H.P. Gerber, R.S. Johnson, G. Bergers, The hypoxic response of tumors is dependent on their microenvironment, Cancer Cell 4 (2003) 133–146, https://doi.org/10.1016/S1535-6108(03)00194-6.
[34] B. Campos, F. Wan, M. Farhadi, A. Ernst, F. Zeppernick, K.E. Tagscherer, R. Ahmadi, J. Lohr, C. Dictus, G. Gdynia, S.E. Combs, V. Goidts, B.M. Helmke, V. Eckstein, W. Roth, P. Beckhove, P. Lichter, A. Unterberg, B. Radlwimmer, C. Herold-Mende, Differentiation therapy exerts antitumor effects on stem-like glioma cells, Clin. Cancer Res. 16 (2010) 2715–2728, https://doi.org/10.1158/1078-0432.CCR-09-1800.
[35] J. Ponten, E. Macintyre, Long term culture of normal and neoplastic human glia, Acta Pathol Microbiol Scand. 74 (1968) 465–486.
[36] L. Agemy, V.R. Kotamraju, D. Friedmann-Morvinski, S. Sharma, K.N. Sugahara, E. Ruoslahti, Proapoptotic peptide-mediated cancer therapy targeted to cell surface p32, Mol. Ther. 21 (2013) 2195–2204, https://doi.org/10.1038/mt.2013.191.
[37] D. Saha, R.L. Martuza, S.D. Rabkin, Macrophage polarization contributes to Glioblastoma eradication by combination Immunovirotherapy and immune checkpoint blockade, Cancer Cell (2017), https://doi.org/10.1016/j.ccell.2017.07.006.
[38] E.M. Kemper, W. Leenders, B. Küsters, S. Lyons, T. Buckle, A. Heerschap, W. Boogerd, J.H. Beijnen, O. van Tellingen, Development of luciferase tagged brain tumour models in mice for chemotherapy intervention studies, Eur. J. Cancer (2006), https://doi.org/10.1016/j.ejca.2006.07.013.
[39] G. Gambarota, W. Leenders, Characterization of tumor vasculature in mouse brain by USPIO contrast-enhanced MRI, Methods Mol. Biol. (2011), https://doi.org/10.1007/978-1-61779-219-9_25.
[40] L. Simón-Gracia, P. Scodeller, S.S. Fuentes, V.G. Vallejo, X. Ríos, E. San Sebastián, V. Sidorenko, D. Di Silvio, M. Suck, F. De Lorenzi, L.Y. Rizzo, S. von Stillfried, K. Kilk, T. Lammers, S.E. Moya, T. Teesalu, Application of polymersomes engineered to target p32 protein for detection of small breast tumors in mice, Oncotarget. (2018), https://doi.org/10.18632/oncotarget.24588.
[41] A. Albanese, P.S. Tang, W.C.W. Chan, The effect of nanoparticle size, shape, and surface chemistry on biological systems, Annu. Rev. Biomed. Eng. (2012), https://doi.org/10.1146/annurev-bioeng-071811-150124.
[42] K. Toome, A.M.A. Willmore, P. Paiste, A. Tobi, K.N. Sugahara, K. Kirsimäe, E. Ruoslahti, G.B. Braun, T. Teesalu, Ratiometric: in vivo auditioning of targeted silver nanoparticles, Nanoscale. (2017), https://doi.org/10.1039/c7nr04056c.
[43] P. Kunkel, U. Ulbricht, P. Bohlen, M.A. Brockmann, R. Fillbrandt, D. Stavrou, M. Westphal, K. Lamszus, Inhibition of glioma angiogenesis and growth in vivo by systemic treatment with a monoclonal antibody against vascular endothelial growth factor receptor-2, Cancer Res. 61 (18) (2001 Sep 15) 6624–6628.
[44] F.J. Wippold, M. Lämmle, F. Anatelli, J. Lennerz, A. Perry, Neuropathology for the neuroradiologist: palisades and pseudopalisades, Am. J. Neuroradiol. (2006), https://doi.org/10.3174/ajnr.A0781.
[45] M. Demeule, J.C. Currie, Y. Bertrand, C. Ché, T. Nguyen, A. Régina, R. Gabathuler, J.P. Castaigne, R. Béliveau, Involvement of the low-density lipoprotein receptor-related protein in the transcytosis of the brain delivery vector Angiopep-2, J. Neurochem. (2008), https://doi.org/10.1111/j.1471-4159.2008.05492.x.
[46] L. Yang, Y. Zhang, Tumor-associated macrophages: from basic research to clinical application, J. Hematol. Oncol. (2017), https://doi.org/10.1186/s13045-017-0430-2.
[47] A. Mantovani, S. Sozzani, M. Locati, P. Allavena, A. Sica, Macrophage polarization: tumor-associated macrophages as a paradigm for polarized M2 mononuclear phagocytes, Trends Immunol. (2002), https://doi.org/10.1016/S1471-4906(02)02302-5.
[48] T. Chanmee, P. Ontong, K. Konno, N. Itano, Tumor-associated macrophages as major players in the tumor microenvironment, Cancers (Basel). (2014), https://doi.org/10.3390/cancers6031670.
[49] J. Hamzah, V.R. Kotamraju, J.W. Seo, L. Agemy, V. Fogal, L.M. Mahakian, D. Peters, L. Roth, M.K.J. Gagnon, K.W. Ferrara, E. Ruoslahti, Specific penetration and accumulation of a homing peptide within atherosclerotic plaques of apolipoprotein E-deficient mice, Proc. Natl. Acad. Sci. (2011), https://doi.org/10.1073/pnas.1104540108.
[50] H.Y. Kim, R. Li, T.S.C. Ng, G. Courties, C.B. Rodell, M. Prytyskach, R.H. Kohler, M.J. Pittet, M. Nahrendorf, R. Weissleder, M.A. Miller, Quantitative imaging of tumor-associated macrophages and their response to therapy using 64 cu-Labeled Macrin, ACS Nano (2018), https://doi.org/10.1021/acsnano.8b04338.
[51] R. Weissleder, G. Elizondo, J. Wittenberg, C.A. Rabito, H.H. Bengele, L. Josephson, Ultrasmall superparamagnetic iron oxide: characterization of a new class of contrast agents for MR imaging, Radiology. (1990), https://doi.org/10.1148/radiology.175.2.2326474.
[52] P. Scodeller, L. Simón-Gracia, S. Kopanchuk, A. Tobi, K. Kilk, P. Säälik, K. Kurm, M.L. Squadrito, V.R. Kotamraju, A. Rinken, M. De Palma, E. Ruoslahti, T. Teesalu, Precision targeting of tumor macrophages with a CD206 binding peptide, Sci. Rep. (2017), https://doi.org/10.1038/s41598-017-14709-x.
[53] Y. Soda, T. Marumoto, D. Friedmann-Morvinski, M. Soda, F. Liu, H. Michiue, S. Pastorino, M. Yang, R.M. Hoffman, S. Kesari, I.M. Verma, Transdifferentiation of glioblastoma cells into vascular endothelial cells, Proc. Natl. Acad. Sci. (2011), https://doi.org/10.1073/pnas.1016030108.
[54] X. Mei, Y.S. Chen, F.R. Chen, S.Y. Xi, Z.P. Chen, Glioblastoma stem cell differentiation into endothelial cells evidenced through live-cell imaging, Neuro-Oncology (2017), https://doi.org/10.1093/neuonc/nox016.
[55] J.J. Vredenburgh, A. Desjardins, J.E. Herndon, J.M. Dowell, D.A. Reardon, J.A. Quinn, J.N. Rich, S. Sathornsumetee, S. Gururangan, M. Wagner, D.D. Bigner, A.H. Friedman, H.S. Friedman, Phase II trial of bevacizumab and irinotecan in recurrent malignant glioma, Clin. Cancer Res. (2007), https://doi.org/10.1158/1078-0432.CCR-06-2309.
[56] M. Pàez-Ribes, E. Allen, J. Hudock, T. Takeda, H. Okuyama, F. Viñals, M. Inoue, G. Bergers, D. Hanahan, O. Casanovas, Antiangiogenic therapy elicits malignant progression of Tumors to increased local invasion and distant metastasis, Cancer Cell (2009), https://doi.org/10.1016/j.ccr.2009.01.027.
[57] V. Yenugonda, N. Nomura, V. Kouznetsova, I. Tsigelny, V. Fogal, E. Nurmemmedov, S. Kesari, I. Babic, A novel small molecule inhibitor of p32 mitochondrial protein overexpressed in glioma, J. Transl. Med. (2017), https://doi.org/10.1186/s12967-017-1312-7.